View Online

Preparation and characterization of lanthanum–gadolinium monazites as ceramics for radioactive waste storage

Olivier Terra,[a] Nicolas Clavier,[a] Nicolas Dacheux*[a] and Renaud Podor[b]

[a] *Groupe de Radiochimie, Institut de Physique Nucléaire, Bât.100, Université Paris-Sud, 91406, Orsay, France. E-mail: dacheux@ipno.in2p3.fr; Fax: +33 1 69 15 71 50; Tel: +33 1 69 15 73 46*

[b] *Laboratoire de Chimie du Solide Minéral (CNRS UMR 7555), Université H. Poincaré-Nancy I, BP 239, 54506, Vandœuvre lès Nancy, France*

Received (in Montpellier, France) 24th December 2002, Accepted 6th February 2003
First published as an Advance Article on the web 15th May 2003

Published on 15 May 2003 on http://pubs.rsc.org | doi:10.1039/B212805P
Downloaded on 26 October 2010

Several $La_{1-x}Gd_xPO_4$ solid solutions were prepared in the monazite- or rhabdophane-type structures for various x values using three methods of preparation (direct evaporation, synthesis in closed PTFE containers on a sand bath or in autoclaves). Samples of rhabdophane-type $La_{1-x}Gd_xPO_4{\cdot}nH_2O$ ($n \approx 0.5$) were prepared at 150 °C only for $x \geq 0.4$. For $x \leq 0.3$, the solids were precipitated as the monazite-type structure. These results were confirmed by the study of pure rare earth phosphates synthesized under the same conditions. By these means, well-crystallized and monophase samples of $MPO_4{\cdot}nH_2O$ ($n \approx 0.5$–1) in the monazite (La, Ce), rhabdophane (Nd, Sm, Eu, Gd, Tb, Dy) or churchite (Ho, Er, Tm, Yb, Lu) forms were prepared.

On the basis of the variation of the specific area *versus* the holding temperature and of the dilatometric studies, the optimal temperature of sintering for these solids was found to be between 1250 and 1400 °C. The effective relative densities of the pellets of $GdPO_4$ prepared using a two-step procedure (pressing between 200 and 700 MPa, then heat treatment at 1300 °C) reached 96% of the value calculated from the XRD data. The chemical durability of sintered samples of $GdPO_4$ was evaluated in several acidic media between room temperature and 90 °C. The very low normalized dissolution rates R_L (between 10^{-6} and 10^{-3} g m^{-2} day^{-1}) measured even in very acidic media confirmed the very good retention properties of this kind of phosphate-based matrix for the immobilization of radionuclides and especially of trivalent actinides.

Introduction

The disposal of nuclear waste in an underground repository is currently considered as a likely option for the immobilization of long-lived radionuclides. One of the main factors that could affect the safety of this type of nuclear waste storage is groundwater infiltration, leading to contact between the matrix and a given solution. Under these conditions, it is necessary to stabilize the radionuclides in solids (*e.g.*, ceramics) of low solubility in order to delay their release into water and finally their migration to the biosphere.

In the field of the immobilization of trivalent and tetravalent actinides, several phosphate matrices such as monazites or brabantites,[1–8] apatites,[9–11] sodium dizirconium phosphate (NZP),[12–15] zirconium phosphates[16,17] or thorium phosphates[18–25] were studied previously, considering several properties of interest such as easy preparation and their sintering and resistance to aqueous corrosion and radiation damage. In this context, we first re-examined the chemistry of uranium and thorium phosphates[18,26–29] in order to propose a new material highly resistant to aqueous corrosion, thorium phosphate diphosphate (TPD), which appeared as a very promising material for the immobilization of tetravalent actinides. Nevertheless, it does not allow the incorporation of large amounts of trivalent actinides (less than 0.5 wt. % of americium or curium). Accordingly, we synthesized several monazites of different compositions with the aim of proceeding finally to the preparation of TPD/monazite-based composites.

The behavior of actinides in monazites was already described by Kelly *et al.* from an oxidation state point of view.[30] Actinide-doped $LnPO_4$ single crystals were grown by means of a flux method and the actinide valence states were determined. Several samples of monazite-type $LaPO_4$ doped with uranium (1.7 wt. %), neptunium (1.5 to 3 wt. %), plutonium (4.3 to 6.0 wt. %), americium (0.2 wt. %) or curium (0.1 to 0.25 wt. %) were prepared. These authors reported that the oxidation states of actinides in these solids were U(IV) and U(III), Np(IV), Pu(IV), Am(III) and Cm(III) which appeared to be a rather curious result for several of these actinides. The preparation of lanthanum phosphate ceramics (monazite-type structure) doped with americium ^{241}Am (which has a high specific activity of 2.1×10^7 Bq g^{-1}), starting from a mixture of lanthanum and americium nitrate solutions in 1 M HNO_3 and concentrated phosphoric acid, was also described by Aloy *et al.*[31] The sintered samples (prepared after hot-pressing at 29.4 MPa, followed by a heat treatment between 900 and 1200 °C) exhibited an apparent density of about 84% and a rather high resistance to dissolution in distilled water at 90 °C, compared to several other matrices such as borosilicate glasses.

The incorporation of large amounts of tetravalent actinides was obtained in the monazite structure by the simultaneous incorporation of calcium, leading to the formation of $CaTh(PO_4)_2$ and $CaU(PO_4)_2$ brabantites.[32] A complete solid solution was found between $CaTh(PO_4)_2$ or $CaU(PO_4)_2$ and $NdPO_4$. Nevertheless, the authors reported that $CaU(PO_4)_2$ was prepared as a pure phase only when firing the samples at 1200 °C under inert conditions. Indeed, this solid was not obtained when heating the powder in air due to the oxidation of U(IV) into U(VI). More recently, crystals of solid solutions of $La_{1-2x}U_xCa_xPO_4$ were prepared with success using

This journal is © The Royal Society of Chemistry and the Centre National de la Recherche Scientifique 2003

View Online

hydrothermal conditions (780 °C, 200 MPa) in the presence of a Ni/NiO buffer in order to control the dioxygen fugacity and to avoid the oxidation of uranium(IV) into uranyl.[2] The unit cell parameters of $La_{1-2x}U_xCa_xPO_4$ decreased linearly from $LaPO_4$ to $Ca_{0.5}U_{0.5}PO_4$ (the last member of the series), which was consistent with the simultaneous replacement of lanthanum [$^{IX}r(La^{3+}) = 1.216$ Å] by calcium [$^{IX}r(Ca^{2+}) = 1.18$ Å] and tetravalent uranium [$^{IX}r(U^{4+}) = 1.05$ Å] in the monazite structure.[33] However, for all the samples, some crystals of $U_2(P_3O_{10})(PO_4)$ (previously denoted as β-UP_2O_7)[34] were coprecipitated as a minor phase with uranium–calcium-bearing monazites. Moreover, samples of composition $CaNp(PO_4)_2$ and $CaNp_{0.7}Pu_{0.3}(PO_4)_2$ were synthesized with success by Tabuteau *et al.* using a mixture of powdered NpO_2, PuO_2, $CaCO_3$ and $(NH_4)_2HPO_4$. In these solids, both actinides were incorporated in the tetravalent state.[35] According to the results of Podor *et al.*,[2,3] the formation of brabantites is driven by the ionic radii of the divalent cation, $\overline{^{IX}r(M^{II})}$, the tetravalent cation, $\overline{^{IX}r(M^{II})}/\overline{^{IX}r(M^{IV})}$, and the average cationic radius, $\overline{^{IX}r(M^{IV+II})}$, in the monazite structure. Indeed, brabantites were prepared under the following conditions: when $1.107\ \text{Å} \leq \overline{^{IX}r(M^{IV+II})} \leq 1.216\ \text{Å}$ and $1.082\ \text{Å} \leq \overline{^{IX}r(M^{II})}/\overline{^{IX}r(M^{IV})} \leq 1.238\ \text{Å}$.

In order to guarantee the good immobilization of actinides in the monazite samples and to avoid their migration to the biosphere, the chemical durability of these materials was also examined. Only a few results are available on the dissolution of monazites. Among them, Boatner *et al.*,[36] reported the dissolution of La(Am)PO_4 crystals (0.5 wt. % of Am_2O_3) in distilled water at 200 °C and 250 psi. They showed that the dissolution of these materials was 295 times lower than borosilicate glasses at room temperature and atmospheric pressure. More recently, an experimental study of the dissolution of natural monazite was developed by Oelkers and Poitrasson[37] as a function of temperature from 50 to 230 °C and for pH values ranging from 1.5 to 10. The steady state dissolution rates varied from 4×10^{-18} to 3×10^{-16} mol cm^{-2} s^{-1} (*i.e.*, 8×10^{-7} to 6×10^{-4} g m^{-2} day^{-1}) at 70 °C, which remained 6 to 8 orders of magnitude lower than that of basaltic glass. Several papers published by Olander and Eyal[38–40] were also devoted to the quantitative modeling of uranium and thorium leaching from monazite in the presence of carbonate ions. The differences in the leaching properties between uranium and thorium (uranium leached more readily than thorium from monazite) persisted throughout sequential leaching tests over 6 to 8 years. This was explained by the different mobilities of both radioelements (uranium having a higher solid-state diffusivity in the near-surface layers of the mineral than thorium). Additionally, since in natural ores monazites have incorporated large amounts of thorium and uranium, they are subject to radiation damage (including damage due to α particles) during their natural lifetime. The conservation of the physical and chemical integrity is evidence of an intrinsic resistance to radiation.

Since the behavior of trivalent actinides (Am, Cm) in phosphate medium is almost the same as that of lanthanides (La, Nd, Gd) and their ionic radii are almost the same, we prepared several lanthanide phosphates as surrogates for americium and curium. We report in this paper the synthesis, using several synthetic methods, and characterization of samples of $La_{1-x}Gd_xPO_4$ (rhabdophane-type and monazite-type structures), in order to obtain sintered lanthanum–gadolinium monazite-type samples and to identify the solubility-controlling phases during the leaching tests of these ceramics. Additionally, these crystallized phases of very low solubility could be used as potential matrices for the decontamination of low-level radioactive liquid waste. With this aim, we also examined their resistance to aqueous corrosion during leaching tests.

Experimental

Synthesis

All the chemicals used during the synthesis and the analysis of the leachates were of "pro-analysis" quality. They were from Aldrich and Fluka. Concentrated solutions of gadolinium and lanthanum (0.6–1.4 M) were prepared in nitric or hydrochloric acids by dissolution of $La(NO_3)_3 \cdot 6H_2O$, $LaCl_3 \cdot 7H_2O$, $Gd(NO_3)_3 \cdot 6H_2O$ or $GdCl_3 \cdot 6H_2O$ salts in the corresponding acid (0.5–1 M). The concentrations of the final solutions were determined using conventional analytical techniques.[41]

Several grams of $La_{1-x}Gd_xPO_4$ (with $x = 0$, 0.2, 0.3, 0.35, 0.4, 0.5, 0.6, 0.65, 0.7, 0.8 and 1) were synthesized starting from a mixture of concentrated phosphoric acid ($C = 5$ M) and lanthanum and/or gadolinium solutions ($C = 0.6$–1.4 M) prepared in 1 M HCl or 0.5 M HNO_3. The mixture was prepared considering the final composition required, that is the following mole ratios: $(La + Gd)/PO_4 = 1$ and $La/Gd = (1-x)/x$. In order to avoid the formation of M_2O_3 (M = La, Gd) as a minor phase after heating at high temperature, an excess of 1 to 2 mol % of phosphoric acid was added to the mixture before the precipitation. In these acidic media, the formation of gelatinous compounds was always avoided.

The precipitation of the solid was performed in three different ways. The first was based on the direct evaporation of the mixture on a sand bath until a dry residue was obtained. The partly crystallized solid obtained was then ground manually, heated at 400 °C for 14 h to eliminate water and the remaining acid, and finally at 1300 °C for 10 to 14 h to improve the crystallization of the monazite. In the second method, the mixture containing the cations and phosphoric acid was put in a closed PTFE container (maximum volume: 23 mL) on a sand bath for 1 to 2 weeks at 150 °C. The third method involved hydrothermal conditions of synthesis. The initial solutions containing the cations and phosphate ions were mixed in a closed PTFE container then put in Parr Instrument Company autoclaves for 1 to 2 months at a constant temperature ranging from 150 to 200 °C. For the two latter synthetic methods, the final precipitate of $La_{1-x}Gd_xPO_4 \cdot nH_2O$ was first filtered, washed, dried, then ground manually, characterized, and finally heated at high temperature in order to obtain samples of $La_{1-x}Gd_xPO_4$ (monazite-type structure). All the solids prepared at 150 °C were compared to several $LnPO_4 \cdot nH_2O$ compounds (Ln = La–Lu) prepared as references. To this aim, 2–10 g of various salts such as $Ce(NO_3)_3 \cdot 6H_2O$, $PrCl_3 \cdot 6H_2O$, Nd_2O_3, Sm_2O_3, $EuCl_3$, TbO_x ($x = 1.5$–2), Dy_2O_3, Ho_2O_3, $ErCl_3 \cdot 6H_2O$, Tm_2O_3, Yb_2O_3 and Lu_2O_3 were digested in closed PTFE containers in a mixture of 2 M HCl or HNO_3 and 5 M H_3PO_4.

Characterization

The high temperature treatments were performed in alumina boats in an ADAMEL FR20 furnace up to 1050 °C or in a PYROX MDB 15 or HM 40 furnace up to 1300 °C with heating rates of 2–5 °C min^{-1}.

X-Ray powder diffraction (XRD) patterns were collected with a Philips PW 1050/70 or an X'Pert-PRO–PW 3040/60 Roentgen diffractometer system using Cu K_α rays ($\lambda = 1.5418$ Å). Several XRD patterns were collected for temperatures ranging from room temperature to 1175 °C. The samples were also characterized by IR absorption spectroscopy. The spectra were recorded from 400 to 4000 cm^{-1} using cylindrical pellets ($Ø = 10$ mm) of 1–2 wt. % in KBr with an Hitachi I-2001 spectrophotometer. TGA and DTA experiments were done with a Setaram TG 92-16 apparatus under inert atmosphere (argon) with a heating rate of 2 °C min^{-1}.

The electron probe microanalyses (EPMA) were carried out using a Cameca SX 50 apparatus with an acceleration voltage

Published on 15 May 2003 on http://pubs.rsc.org | doi:10.1039/B212805P
Downloaded on 26 October 2010

View Online

of 15 kV and a current of 10 nA considering the following calibration standards: synthetic $LaPO_4$ (L_α ray of lanthanum and K_α ray of phosphorus) and GdTiGe (L_α ray of gadolinium)†.

The grain size distribution of the powdered samples was determined with a Coulter LS 230 laser particle size apparatus while the specific area was measured with a Coulter SA 3100 apparatus using the B.E.T. method (nitrogen adsorption at 77 K).[42] SEM micrographs were carried out with a Philips XL30 scanning electron microscope.

Sintering

The sintered samples of $La_{1-x}Gd_xPO_4$ (monazite-type structure) were obtained using uniaxial pressing at room temperature followed by heat treatment at 1250 or 1300 °C. The initial pressing was performed between 100 and 700 MPa with a Graseby/Specac press supplied by Eurolab and using tungsten carbide dies purchased from Siametir in order to get rectangular pellets ($5 \times 5 \times 20$ or $3 \times 3 \times 10$ mm^3). The dilatometer was a TMA 92-16 apparatus from Setaram working under argon atmosphere from room temperature to 1400 °C for our experiments with heating rates of 5 °C min^{-1} for heating and 20 °C min^{-1} for cooling. The density of the sintered samples was measured at room temperature using water ($\rho = 0.997$ g cm^{-3} at 25 °C) and/or helium pycnometry (for these experiments, a Multi pycnometer from Quantachrome was used).

Leaching test procedure and analysis of the leachate

High density polyethylene (HDPE) containers were chosen in order to perform the leaching experiments at room temperature while PTFE vessels were preferred for experiments above 70 °C. We checked that, under the conditions of the leaching tests, less than 1% of the total dissolved elements was adsorbed onto the surface of the containers.

Prior to the leaching experiments, all the samples were washed in order to avoid any perturbation due to the presence of crystal defects, minor phases or small particles, which could produce, for instance, some colloids during the first days of the leaching tests. This washing step was performed at 25 or 50 °C for 1 to 7 days in 10^{-1} M HNO_3 or HCl. For each dissolution curve, the leaching tests were performed between room temperature and 90 °C by mixing 200 mg of sintered sample with 5 mL of acidic solution. In order to have a better understanding of the kinetic law of the dissolution process and to increase the normalized dissolution rates, all the leaching tests were performed in acidic media (10^{-1}–10^{-4} M HNO_3 or HCl).

At regular intervals, a small volume of the leachate (100 μL) was removed, then renewed by fresh solution. We considered that, under these conditions, the solution–solid system was not significantly modified. Before each measurement, the leachate was centrifugated at 13 000 rpm for 15 min in order to avoid the presence of colloids and small particles in the analyzed solution. The concentration of gadolinium was determined in the leachate by inductively coupled plasma mass spectrometry using a Fisons Plasma Quad apparatus. Prior to performing the determination of the gadolinium concentration, the sample was diluted, then terbium and bismuth were added up to 1 ppb each as an internal monitor. The final values reported are an average of four determinations. From these results, the normalized leaching N_L (expressed in g m^{-2}) was calculated from the following equation:

$$N_L = \frac{C_{Gd} \times V \times M_{Gd}}{x_{Gd} \times S} \quad (1)$$

† PIXE experiments were performed with a Tandem-type accelerator using 3 MeV proton beam. For these analyses, samples were first shaped in pellet form using an uniaxial pressing at 300 MPa.

where C_{Gd} is the concentration of gadolinium in the leachate (mol L^{-1}) determined from the ^{160}Gd isotope (22% natural occurrence), V is the volume of leachate (L), x_{Gd} is the mass ratio of gadolinium in the solid and S (m^2) is the effective surface of contact between the solid and the solution. Thus, the corresponding normalized dissolution rate R_L (expressed g m^{-2} day^{-1}) was determined from the evolution of the normalized leaching as follows:

$$R_L = \frac{d N_L}{dt} \quad (2)$$

Results and discussion

Characterization of the solids

PIXE and EPMA studies. The chemical composition and homogeneity of the powdered lanthanum–gadolinium phosphate samples prepared using precipitation or hydrothermal conditions were verified by particle-induced X-ray electron (PIXE) and/or electron probe microanalysis (EPMA) for several heating temperatures. The results obtained on the samples heated at 1300 °C are collected in Table 1. All the solids appeared homogeneous and single phase. The experimental elementary weight percents are consistent with that expected. Moreover, the mole ratios $(La + Gd)/PO_4$ remained equal to 1 while the La/Gd mole ratios varied as expected from the general formulae $La_{1-x}Gd_xPO_4$. For two compositions, $GdPO_4$ and $La_{0.5}Gd_{0.5}PO_4$, some EPMA experiments were also performed on samples heated at several temperatures ranging from 500 to 1300 °C (Table 2). These results showed that the mole ratios $(La + Gd)/PO_4$ remained close to 1 irrespective of the temperature used. However, the excess of phosphate initially present in the mixture in order to avoid the formation of lanthanum and gadolinium oxides was eliminated by heating between 700 and 1000 °C. For all the temperatures studied, no secondary phases such as $M(PO_3)_3$, $M_4(P_2O_7)_3$, $(MO)_3(PO_4)$ or M_2O_3 (M = La or Gd) were observed in the mixtures.

XRD and IR spectroscopy. The XRD patterns of $La_{1-x}Gd_xPO_4$, prepared by precipitation in closed PTFE containers at 150 °C, were compared to that recorded for several rare earth cations (Ln = Ce, Pr, Nd, Sm, Eu, Tb, Dy, Ho, Er, Tm, Yb and Lu) prepared under the same conditions. The crystallographic data of all the solids synthesized by this method are reported in Table 3. Two kinds of $La_{1-x}Gd_xPO_4{\cdot}nH_2O$ solids were prepared, depending on the initial La/Gd mole ratio considered (Fig. 1). For $x \leq 0.3$, the solids were precipitated as monazites (monoclinic system, space group $P2_1/n$) while for $x \geq 0.4$, the precipitation of rhabdophanes (hexagonal system, space group $P3_121$) was observed. For $x = 0.35$, a mixture of monazite and rhabdophane was obtained. This different behavior was correlated to the average ionic radius of the trivalent cations in the structure. Indeed, for $La_{1-x}Gd_xPO_4{\cdot}nH_2O$ samples, monazite was precipitated for $\overline{^{VIII}r(Ln^{3+})} \geq 1.128$ Å while rhabdophane-type was obtained for $\overline{^{VIII}r(Ln^{3+})} \leq 1.117$ Å, the mixture being obtained for $\overline{^{VIII}r(Ln^{3+})} = 1.122$ Å. On the basis of the refined unit cell parameters (Table 3), this mixture consisted of the monazite having the composition $La_{0.77}Gd_{0.23}PO_4$ [$\overline{^{VIII}r(Ln^{3+})} = 1.135$ Å] and the rhabdophane $La_{0.58}Gd_{0.42}PO_4{\cdot}nH_2O$ [$\overline{^{VIII}r(Ln^{3+})} = 1.115$ Å]. These results were then correlated to those obtained for the phosphates of the other rare earth cations studied. Monazite-type phosphates were only precipitated for lanthanum [$^{VIII}r(La^{3+}) = 1.160$ Å] and cerium [$^{VIII}r(Ce^{3+}) = 1.143$ Å] while rhabdophane-type phosphates were obtained from neodymium to dysprosium [1.027

Published on 15 May 2003 on http://pubs.rsc.org | doi:10.1039/B212805P
Downloaded on 26 October 2010

View Online

Table 1 Results of PIXE and EPMA analyses of $La_{1-x}Gd_xPO_4$ powdered samples ($\theta = 1300\,^{\circ}C$)

Sample	Gd/wt. %	La/wt. %	P/wt. %	(La + Gd)/P	La/Gd
$LaPO_4$					
Calcd	–	59.4	13.2	1.00	–
PIXE	–	58.6 ± 2.1	13.7 ± 0.5	0.95 ± 0.06	–
EPMA	–	58.9 ± 1.0	13.3 ± 0.3	0.99 ± 0.03	–
$La_{0.80}Gd_{0.20}PO_4$					
Calcd	13.2	46.8	13.0	1.00	4.00
PIXE	13.5 ± 0.5	44.2 ± 2.1	13.9 ± 0.7	0.90 ± 0.11	3.70 ± 0.32
EPMA	14.5 ± 0.9	45.6 ± 1.1	13.1 ± 0.3	0.99 ± 0.02	3.60 ± 0.27
$La_{0.65}Gd_{0.35}PO_4$					
Calcd	22.9	37.6	12.9	1.00	1.86
PIXE	23.0 ± 0.9	35.8 ± 1.4	13.4 ± 0.6	0.93 ± 0.11	1.76 ± 0.14
EPMA	23.9 ± 0.6	36.6 ± 1.1	12.9 ± 0.4	1.00 ± 0.03	1.73 ± 0.06
$La_{0.50}Gd_{0.50}PO_4$					
Calcd	32.3	28.6	12.8	1.00	1.00
PIXE	31.8 ± 0.8	28.4 ± 0.7	13.1 ± 0.3	0.93 ± 0.05	1.00 ± 0.05
EPMA	31.6 ± 1.6	29.1 ± 1.5	12.9 ± 0.6	0.99 ± 0.02	1.05 ± 0.10
$La_{0.35}Gd_{0.65}PO_4$					
Calcd	41.5	19.8	12.6	1.00	0.54
PIXE	40.8 ± 1.4	18.3 ± 0.7	13.5 ± 0.3	0.89 ± 0.09	0.51 ± 0.04
EPMA	40.9 ± 1.0	19.9 ± 0.8	12.9 ± 0.2	0.97 ± 0.02	0.55 ± 0.04
$La_{0.20}Gd_{0.80}PO_4$					
Calcd	50.6	11.2	12.5	1.00	0.25
PIXE	49.8 ± 2.0	10.2 ± 0.4	13.3 ± 0.5	0.91 ± 0.11	0.23 ± 0.02
EPMA	49.9 ± 0.6	11.4 ± 1.6	12.7 ± 0.4	0.97 ± 0.02	0.26 ± 0.01
$GdPO_4$					
Calcd	62.3	–	12.3	1.00	–
PIXE	61.8 ± 2.4	–	12.7 ± 0.5	0.96 ± 0.05	–
EPMA	62.2 ± 1.6	–	12.3 ± 0.3	1.00 ± 0.04	–

Published on 15 May 2003 on http://pubs.rsc.org | doi:10.1039/B212805P
Downloaded on 26 October 2010

Å $\leq {}^{VIII}r(Ln^{3+}) \leq$ 1.109 Å]. As already found for $La_{0.65}Gd_{0.35}PO_4{\cdot}nH_2O$ [$^{VIII}r(Ln^{3+})$ = 1.122 Å], a mixture of rhabdophane and monazite structures was always obtained for praseodymium [$^{VIII}r(Pr^{3+})$ = 1.126 Å]. Finally, for the smaller rare earth cations [Ho–Lu; 0.977 Å $\leq {}^{VIII}r(Ln^{3+}) \leq$ 1.015 Å], the solids as precipitated presented the tetragonal system of churchite-type structure as expected from the literature.[43–46]

For pattern indexing, the precise determination of the peak positions of $La_{1-x}Gd_xPO_4{\cdot}nH_2O$ was carried out using the fitting program EVA, available in the software package Diffrac-AT V 3.0, purchased from Socabim and supplied by Siemens. Silicon (JCPDS file n° 27-1402)[47] was added as an internal monitor. The unit cell parameters of $MPO_4{\cdot}nH_2O$ (monazite-, rhabdophane- and churchite-type structures) were refined using the U-Fit program[48] considering the space groups reported in the literature ($P2_1/n$, $P3_121$ and $I4_1/amd$, respectively).[49,50] The values determined (Table 3) were in good agreement with those reported for $LaPO_4$[44] and $CePO_4$[51] monazite-type structures, for $NdPO_4{\cdot}0.5H_2O$[52,53] $SmPO_4{\cdot}0.5H_2O$,[52] $EuPO_4{\cdot}H_2O$,[45] $GdPO_4{\cdot}H_2O$,[49] $TbPO_4{\cdot}H_2O$ and $DyPO_4{\cdot}1.5H_2O$[45] rhabdophane-type structures, and for $HoPO_4{\cdot}3H_2O$, $ErPO_4{\cdot}3H_2O$, $TmPO_4{\cdot}3H_2O$, $YbPO_4{\cdot}3H_2O$ and $LuPO_4{\cdot}3H_2O$ churchite-type structures.[45,54] For $La_{1-x}Gd_xPO_4{\cdot}nH_2O$ samples, the unit cell parameters decreased linearly with increasing x value, which agrees well with the replacement of lanthanum by gadolinium in the structure. Moreover, the average FWHM values (0.18°) of the XRD lines of $La_{1-x}Gd_xPO_4{\cdot}nH_2O$ did not increase significantly in comparison to those of $GdPO_4{\cdot}nH_2O$ (0.16°). Both observations are consistent with the preparation of solid solutions of $La_{1-x}Gd_xPO_4{\cdot}nH_2O$ in the rhabdophane-type structure for $x \geq 0.4$ and in the monazite-type structure for $x \leq 0.3$.

Table 2 Results of EPMA analysis of $GdPO_4$ and $La_{0.5}Gd_{0.5}PO_4$ *versus* holding temperature

Sample	Gd/wt. %	La/wt. %	P/wt. %	O/wt. %	La/Gd	(La + Gd)/P
$GdPO_4$						
Calcd	62.3	–	12.3	25.4	–	1.00
500 °C	60.9 ± 0.9	–	13.0 ± 0.4	26.1 ± 0.6	–	0.93 ± 0.04
700 °C	61.2 ± 1.7	–	12.9 ± 0.3	26.0 ± 0.4	–	0.94 ± 0.03
1000 °C	62.0 ± 2.5	–	12.5 ± 0.4	25.6 ± 0.9	–	0.98 ± 0.02
1200 °C	61.9 ± 1.9	–	12.5 ± 0.4	25.6 ± 0.7	–	0.98 ± 0.04
1250 °C	62.3 ± 1.7	–	12.3 ± 0.4	25.4 ± 0.7	–	1.00 ± 0.03
1300 °C	62.2 ± 1.6	–	12.3 ± 0.3	25.4 ± 0.6	–	1.00 ± 0.03
$La_{0.50}Gd_{0.50}PO_4$						
Calcd	32.3	28.6	12.8	26.3	1.00	1.00
500 °C	31.7 ± 2.1	27.9 ± 2.0	13.3 ± 0.8	26.9 ± 1.7	1.01 ± 0.07	0.93 ± 0.03
700 °C	31.0 ± 3.0	29.3 ± 1.5	13.1 ± 0.3	26.7 ± 1.0	1.08 ± 0.09	0.97 ± 0.04
1000 °C	30.8 ± 3.8	29.6 ± 3.8	13.0 ± 1.2	26.7 ± 2.7	1.09 ± 0.12	0.97 ± 0.02
1200 °C	30.7 ± 1.9	29.5 ± 2.5	13.1 ± 1.0	26.8 ± 2.3	1.09 ± 0.14	0.96 ± 0.02
1250 °C	33.0 ± 1.9	27.8 ± 1.9	12.8 ± 0.2	26.4 ± 0.3	0.97 ± 0.12	1.00 ± 0.03
1300 °C	32.0 ± 1.6	28.6 ± 2.1	12.7 ± 0.3	26.3 ± 0.9	1.02 ± 0.12	0.98 ± 0.04

View Online

Published on 15 May 2003 on http://pubs.rsc.org | doi:10.1039/B212805P
Downloaded on 26 October 2010

Table 3 Solids prepared at 150 °C in closed PTFE containers

Compound	Type	$^{VIII}r(Ln^{3+})$[33]	a/Å	b/Å	c/Å	β/°	V/Å^3	Ref.
$LaPO_4$	Mon.	1.160	6.841(2)	7.079(3)	6.508(4)	103.33(7)	306.7(4)	[a]
			6.8313(1)	*7.0705(9)*	*6.5034(9)*	*103.27(1)*	*305.7*	
$CePO_4$	Mon.	1.143	6.803(3)	7.030(3)	6.472(4)	103.60(4)	300.8(4)	[a]
			6.8004(11)	*7.0231(13)*	*6.4717(1)*	*104.46(16)*	*300.6*	51
$NdPO_4$	Rhab.	1.109	7.014(3)	–	6.401(4)	–	272.4(4)	[a]
			7.03	–	*6.39*	–	*273.5*	52,53
$SmPO_4$	Rhab.	1.079	6.9369(7)	–	6.344(1)	–	264.4(1)	[a]
			6.95	–	*6.32*	–	*264.4*	52
$EuPO_4$	Rhab.	1.066	6.920(2)	–	6.342(3)	–	263.0(2)	[a]
			6.91	–	*6.34*	–	*262.2*	45
$GdPO_4$	Rhab.	1.053	6.9055(8)	–	6.323(1)	–	261.1(1)	[a]
			6.9055(2)	–	*6.3257(2)*	–	*261.2*	49
$TbPO_4$	Rhab.	1.040	6.868(2)	–	6.325(6)	–	258.4(4)	[a]
			6.87	–	*6.33*	–	*258.7*	45
$DyPO_4$	Rhab.	1.027	6.844(2)	–	6.290(2)	–	255.1(2)	[a]
			6.80	–	*6.29*	–	*251.9*	45
$HoPO_4$	Church.	1.015	6.8971(8)	–	6.0427(9)	–	287.4(1)	[a]
			6.89	–	*6.01*	–	*285.3*	45
$ErPO_4$	Church.	1.004	6.864(2)	–	6.014(2)	–	283.3(3)	[a]
			6.89	–	*6.01*	–	*285.3*	45
$TmPO_4$	Church.	0.994	6.8468(7)	–	5.997(1)	–	281.1(2)	[a]
			6.839(1)	–	*5.986(1)*	–	*280.0*	43
$YbPO_4$	Church.	0.985	6.832(1)	–	5.981(2)	–	279.2(2)	[a]
			6.84	–	*5.99*	–	*280.2*	45,54
$LuPO_4$	Church.	0.977	6.806(2)	–	5.957(2)	–	275.9(3)	[a]
			6.81	–	*5.95*	–	*275.9*	45
$La_{0.7}Gd_{0.3}PO_4$	Mon.	1.128[b]	6.797(1)	7.015(2)	6.452(3)	103.60(3)	299.0(3)	[a]
$La_{0.65}Gd_{0.35}PO_4$	Mon. and rhab.	1.122[b]	6.806(9)	7.020(5)	6.467(8)	103.61(7)	300.3(9)	[a]
			7.026(1)	–	6.420(1)	–	274.4(1)	[a]
$La_{0.6}Gd_{0.4}PO_4$	Rhab.	1.117[b]	7.042(2)	–	6.447(5)	–	276.9(4)	[a]
$La_{0.5}Gd_{0.5}PO_4$	Rhab.	1.107[b]	7.007(2)	–	6.401(3)	–	272.2(3)	[a]

[a] This work. [b] $\overline{^{VIII}r(Ln^{3+})}$.

Powdered samples of $La_{1-x}Gd_xPO_4$ were also characterized using XRD *versus* holding temperature from room temperature to 1175 °C. The variation of the XRD pattern with the heating temperature is presented in Fig. 2 for $GdPO_4$ (the same study was simultaneously developed for $La_{0.5}Gd_{0.5}PO_4$ and $LaPO_4$). As already discussed, the XRD patterns of $GdPO_4{\cdot}nH_2O$ and $La_{0.5}Gd_{0.5}PO_4{\cdot}nH_2O$ prepared at 150 °C revealed that both solids crystallized in a hexagonal system (rhabdophane-type structure) while lanthanum phosphate initially crystallized in the monazite-type structure. For $GdPO_4{\cdot}nH_2O$ and $La_{0.5}Gd_{0.5}PO_4{\cdot}nH_2O$, the rhabdophane-type structure was maintained up to 700–800 °C, irrespective

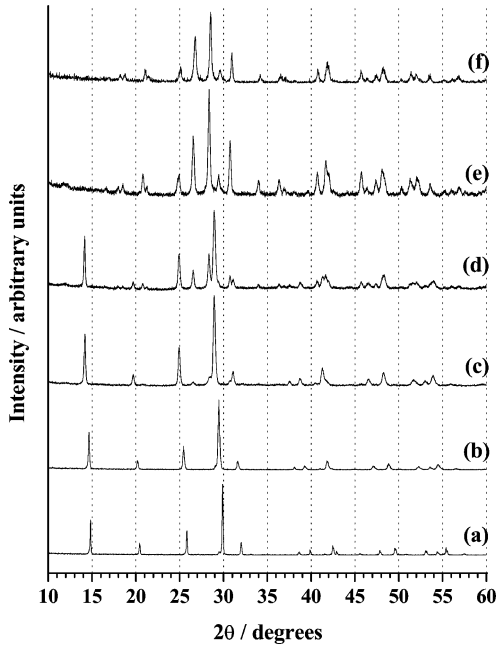

Fig. 1 XRD patterns of $La_{1-x}Gd_xPO_4{\cdot}nH_2O$ with $x = 1$ (a), 0.5 (b), 0.4 (c), 0.35 (d), 0.3 (e) and 0 (f).

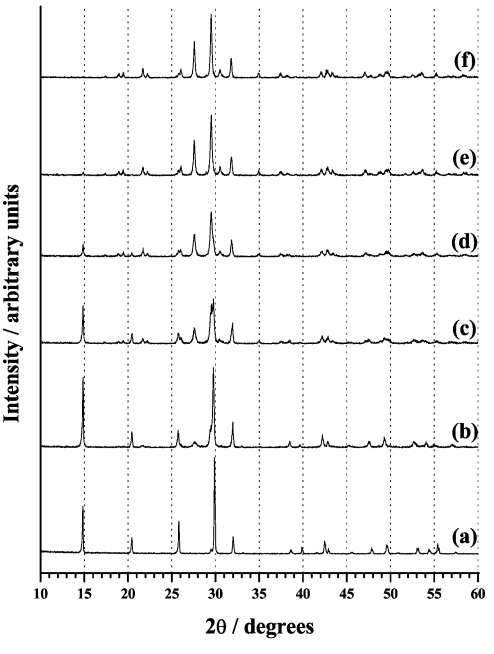

Fig. 2 XRD patterns of $GdPO_4$ at a heating temperature of 25 (a), 800 (b), 850 (c), 900 (d), 1000 (e) and 1175 (f) °C.

View Online

Published on 15 May 2003 on http://pubs.rsc.org | doi:10.1039/B212805P
Downloaded on 26 October 2010

of the synthetic method employed, which is consistent with the literature.[55] Above these temperatures, $GdPO_4$ and $La_{0.5}Gd_{0.5}PO_4$ (rhab.) began to transform into the monazite-type structure. This reaction was complete above 1000 and 900 °C, respectively. According to the literature, $GdPO_4$ (rhab.) should be transformed into $GdPO_4$ (mon.) at 800 °C.[55] This small shift in the phase change temperature could be explained by the differences in the preparation of the samples. For lanthanum phosphate, the transformation $LaPO_4$ (rhab.) → $LaPO_4$ (mon.) was not observed in our conditions of precipitation since the XRD pattern of the monazite-type structure was found to be unchanged between 150 °C and 1175 °C (only the degree of crystallinity was modified when increasing the temperature). This is consistent with the results reported by Jonasson and Vance[55] but does not agree with those of Onoda *et al.*[56] who reported the formation of a mixture of both structures after heating at 150 °C for 20 h starting from a mixture of $La(NO_3)_3{\cdot}9H_2O$ and H_3PO_4. However, according to their results, the rhabdophane form was not formed when using $(NH_4)_2HPO_4$ as the phosphating reagent, whatever the initial lanthanum salt used (sulfate, oxalate, fluoride and oxide). Our series of experiments revealed that the rhabdophane-type structure was rapidly precipitated at 60 and 90 °C in closed PTFE containers while the monazite-type structure was prepared at 150 °C. Complementary syntheses between 100 and 150 °C are now under progress.

We followed the dehydration of $GdPO_4{\cdot}nH_2O$ and $La_{0.5}Gd_{0.5}PO_4{\cdot}nH_2O$ from room temperature to 1300 °C by means of TGA and DTA experiments. For both solids, the weight loss was mainly observed between 100 and 220 °C, which is consistent with literature.[55,57,58] The total weight losses between room temperature and 1300 °C, corresponding to the following reaction:

$$La_{1-x}Gd_xPO_4{\cdot}nH_2O\ (\text{rhab.}) \rightarrow La_{1-x}Gd_xPO_4\ (\text{mon.}) + nH_2O\ \uparrow \quad (3)$$

were found to 3.8 and 3.3 wt. % for $GdPO_4{\cdot}nH_2O$ and $La_{0.5}Gd_{0.5}PO_4{\cdot}nH_2O$, respectively. The corresponding number of water molecules per unit formula is then 0.55 and 0.46, respectively. For both compositions, the solids precipitated in our operating conditions were thus $La_{1-x}Gd_xPO_4{\cdot}0.5H_2O$, which appears to be in good agreement with the literature where the formation of $LnPO_4{\cdot}0.5$–$0.7H_2O$ (Ln = La – Dy) is reported.[45,52,59,60] However, we did not observe in the DTA curve the small exothermic peak assigned by Jonasson and Vance[55] to the transformation of rhabdophane into monazite between 700 and 900 °C.

For all the compositions studied, the $La_{1-x}Gd_xPO_4$ monazite-type samples were prepared after heating above 1000 °C. The FWHM of the XRD lines were determined for $LaPO_4$, $GdPO_4$ and $La_{0.5}Gd_{0.5}PO_4$. It decreased significantly between 700 and 1300 °C, the crystallization being optimal at this latter temperature. The $P2_1/n$ space group of $LaPO_4$ (JCPDS file numbers 32-0493 and 84-0600) and $GdPO_4$ (JCPDS file numbers 32-0386 and 84-0920) was used for pattern indexing of $La_{1-x}Gd_xPO_4$.[47] The unit cell parameters and volume obtained for the seven compositions studied are summarized in Table 4. As the ionic radii of lanthanum and gadolinium in the nine-fold coordination (corresponding to the environment of the cation in the monazite structure) are equal to 1.216 and 1.107 Å, respectively,[33] the substitution of lanthanum by gadolinium in the structure should lead to a decrease of the unit cell parameters (Fig. 3). The values of the four parameters and volume are listed in Table 5 *versus* the substitution ratio, x, on the one hand, and *versus* the average ionic radius, defined as:

$$\overline{^{IX}r_{cat}} = (1-x)\,.^{IX}r_{La} + x\,.^{IX}r_{Gd} \quad (4)$$

on the other hand.[33] It is clear that solid solutions of $La_{1-x}Gd_xPO_4$ were prepared as pure phases at high temperature using all methods of synthesis as already suggested by the EPMA and PIXE experiments. For all the samples, the values of the density determined using helium pycnometry (Table 4) agree well with those calculated from the XRD data and with those reported in the literature for $LaPO_4$ (5.07–5.11) and for $GdPO_4$ (5.99–6.06).[47] In these conditions, the contraction of the unit cell is equal to 2.8%, 3.3%, and 2.5% along a, b and c, respectively, from $LaPO_4$ to $GdPO_4$, which corresponds to a contraction of the unit cell volume of 8.7% and a density increase of about 20%.

All the solid solutions of $La_{1-x}Gd_xPO_4$ prepared were simultaneously characterized using IR spectroscopy. For all the samples, the vibrations corresponding to water molecules (3600 and 1620–1640 cm^{-1}) were observed for heating temperature below 900 °C, which is in good agreement with the preparation of hydrated $La_{1-x}Gd_xPO_4{\cdot}0.5H_2O$. At this stage of the discussion, it is important to consider the presence (or not) of water molecules in the samples analyzed. Indeed, according to the TGA and DTA experiments, the anhydrous solids were probably prepared when heating above 250 °C. However, the observation of the water vibrations in the IR spectra is probably due to the hygroscopic behavior of the samples (water molecules were considered as zeolithic from literature).[57–60] In the IR spectra, we verified that only the bands corresponding to the P–O edge of the PO_4 group were observed [ν_{as}(P–O): 990–1120 cm^{-1}, ν_s(P–O): 960–970 cm^{-1} and δ_{as}(P–O): 540–620 cm^{-1}]. No additional bands that could be assigned to the P–O–P bridge of the P_2O_7 group [ν_s(P–O–P) near 700 cm^{-1} and ν_{as}(P–O–P) near 920 cm^{-1}] were detected. All these spectra are consistent with those reported by Zaki *et al.*[61] and Onoda *et al.*[56]

Determination of the specific area of the samples. In order to determine the best conditions of the preparation of sintered samples, the variation of the specific area was followed *versus* the heating temperature for $LaPO_4$, $La_{0.5}Gd_{0.5}PO_4$ and $GdPO_4$. The results are reported in Fig. 4. For the three solids, the specific area decreased significantly when heated above 800 °C, which is mainly due to an increase of the average grain size by coalescence and to the reduction of the global porosity.

Table 4 Unit cell parameters and volume of $La_{1-x}Gd_xPO_4$ (θ = 1300 °C)

	x						
	0	0.2	0.35	0.5	0.65	0.8	1
a/Å	6.837(1)	6.786(6)	6.765(3)	6.737(4)	6.720(4)	6.684(7)	6.653(2)
b/Å	7.078(2)	7.013(5)	6.990(4)	6.947(3)	6.925(4)	6.883(7)	6.847(2)
c/Å	6.507(2)	6.457(6)	6.448(3)	6.408(4)	6.393(3)	6.353(6)	6.331(2)
β/°	103.28(2)	103.42(4)	103.66(4)	103.69(5)	103.76(9)	103.84(5)	103.96(2)
V/Å^3	306.5(2)	298.9(8)	296.2(6)	291.3(5)	288.8(4)	283.8(8)	279.9(2)
d_{calcd}	5.08 ± 0.02	5.28 ± 0.02	5.39 ± 0.01	5.55 ± 0.02	5.65 ± 0.01	5.82 ± 0.02	5.99 ± 0.02
$d_{meas.}$	5.03 ± 0.02	5.28 ± 0.01	5.39 ± 0.02	5.56 ± 0.04	5.64 ± 0.04	5.77 ± 0.04	6.07 ± 0.04

View Online

Published on 15 May 2003 on http://pubs.rsc.org | doi:10.1039/B212805P
Downloaded on 26 October 2010

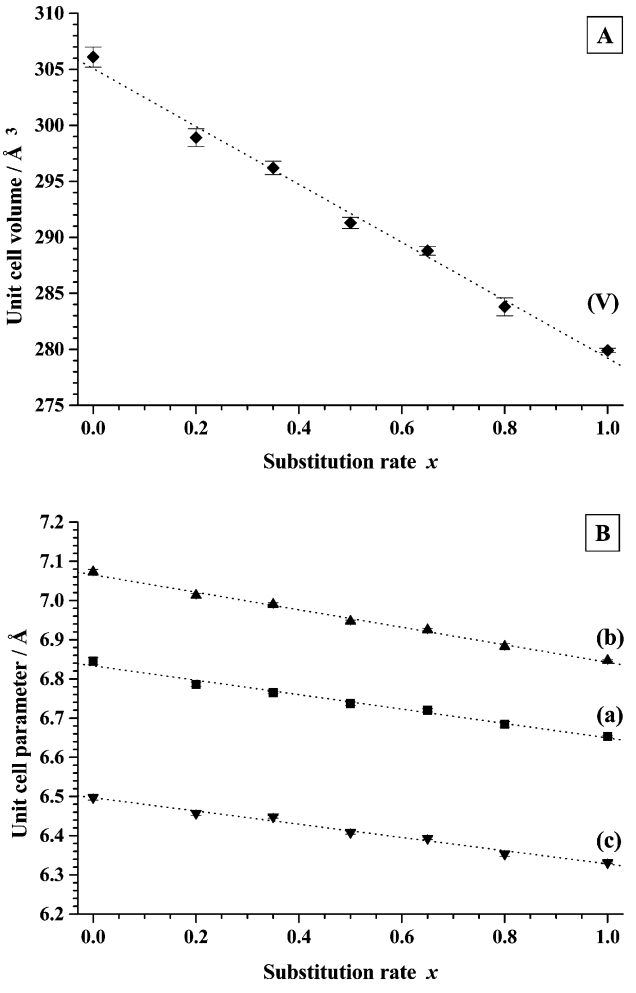

Fig. 3 Variation of (A) the ionic cell volume (◆) and (B) the unit cell parameters: a (■), b (▲) and c (▼) of $La_{1-x}Gd_xPO_4$ *versus* the substitution amount x.

This was confirmed by the observation of these samples by SEM. For $LaPO_4$, the specific area was systematically found to be higher, which is probably due to the initial conditions of preparation (more rapid precipitation during the evaporation step). More generally, the variation of the specific area *versus* the holding temperature led us to conclude that sintering of monazite should be better when firing the samples at temperatures higher than 1250 °C.

Observation of the powdered samples by SEM. Several samples were observed by SEM. Micrographs of gadolinium phosphate prepared at room temperature and heated at 500 and 1300 °C are presented in Fig. 5. The powder prepared at 150° C or heated at 500 °C exhibits needle-like crystals of 1–10 μm in length and 0.5–2 μm in width, characteristic of

Table 5 Variation of unit cell parameters of the solid solutions $La_{1-x}Gd_xPO_4$ *versus* the substitution amount x and the average ionic radius

Unit cell parameter	Variation *versus*	
	x	$\overline{^{IX}r(cat)}$
a/Å	$6.833(6) - 0.18(1)\cdot x$	$4.78(8) + 1.68(7)\cdot\overline{^{IX}r(cat)}$
b/Å	$7.066(5) - 0.22(1)\cdot x$	$4.56(7) + 2.06(6)\cdot\overline{^{IX}r(cat)}$
c/Å	$6.497(5) - 0.17(1)\cdot x$	$4.64(8) + 1.52(7)\cdot\overline{^{IX}r(cat)}$
β/°	$103.29(2) + 0.70(4)\cdot x$	$111.5(5) - 6.7(4)\cdot\overline{^{IX}r(cat)}$
V/Å^3	$305.1(6) - 25.9(9)\cdot x$	$18(8) + 236(7)\cdot\overline{^{IX}r(cat)}$

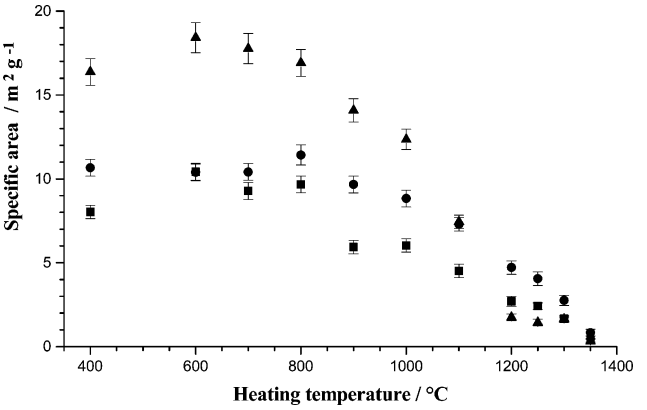

Fig. 4 Variation of the specific area of $LaPO_4$ (▲), $La_{0.5}Gd_{0.5}PO_4$ (●) and $GdPO_4$ (■) *versus* the heating temperature.

the rhabdophane structure [the hexagonal section was clearly observed in Figs. 5(a) and 5(b)]. This morphology was confirmed by the granulometric studies, which revealed the presence of grains of 1–10 μm diameter with an average grain size of about 5 μm. This average grain size did not increase significantly at 1300 °C compared to that observed at room temperature and after heating at 500 °C. Several aggregates of small spherical grains of about 0.1 μm diameter were also observed. From granulometric study, the grain size ranged from 1 to 20 μm (average grain size of 5–10 μm). At this

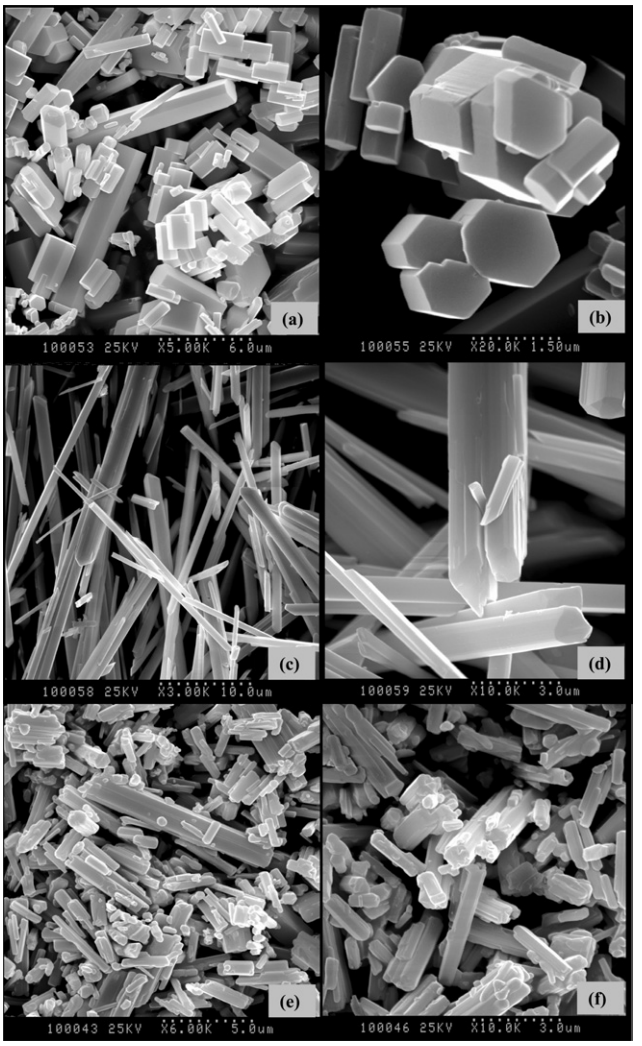

Fig. 5 SEM micrographs of powdered samples of $GdPO_4$ prepared at 150 °C (a,b) and after heating at 500 °C (c,d) or at 1250 °C (e,f).

View Online

holding temperature, the intragranular porosity remained high and was probably responsible for the high specific area, SA, measured (SA = 2–5 $m^2\ g^{-1}$) compared to that determined for several other phosphate materials such as thorium phosphate diphosphate (SA = 0.2–0.4 $m^2 g^{-1}$ for $\theta = 1250\,^{\circ}C$),[62] britholites $Ca_9Nd(PO_4)_5(SiO_4)F_2$ (SA = 0.1–0.3 $m^2\ g^{-1}$ for $\theta = 1390\,^{\circ}C$) or dizirconium oxide phosphate $Zr_2O(PO_4)_2$ (SA = 0.9 $m^2\ g^{-1}$ for $\theta = 1280\,^{\circ}C$).[17] The same morphology was observed on powdered lanthanum–gadolinium phosphate solid solutions after heating at 1250 °C for 12 h.

Preliminary results concerning the sintering of $La_{1-x}Gd_xPO_4$ monazites

Dilatometry study. In order to proceed to the preparation of sintered samples of monazite from rhabdophane under good conditions, we studied the shrinkage of several $La_{1-x}Gd_xPO_4$ samples from room temperature to 1400 °C. The results obtained for $GdPO_4$ and $La_{0.5}Gd_{0.5}PO_4$ are presented in Fig. 6. From this study, it is clear that the shrinkage occurs in two steps. The first, centered at 860 and 810 °C for $GdPO_4$ and $La_{0.5}Gd_{0.5}PO_4$, respectively, was assigned to the transformation of the rabdophane-type structure. This phenomenum, more observable in the $GdPO_4$ sample, was spread over the range of 750 to 950 °C and from 700 to 900 °C, for the Gd and La–Gd samples, respectively. The second step, observed at higher temperature ($\theta \geq 1000\,^{\circ}C$) and continuing up to 1400 °C, was mainly assigned to the swelling of the grains and to the sintering of the samples (this is correlated to the significant decrease of the specific area of the powdered samples in this temperature range). These results are consistent with those of Petek *et al.* who investigated the sintering by continuous reading dilatometry and concluded that the sintering began at 800 °C.[5] On the basis of this dilatometric study, the sintering was achieved by holding the temperature at a value higher than 1250 °C.

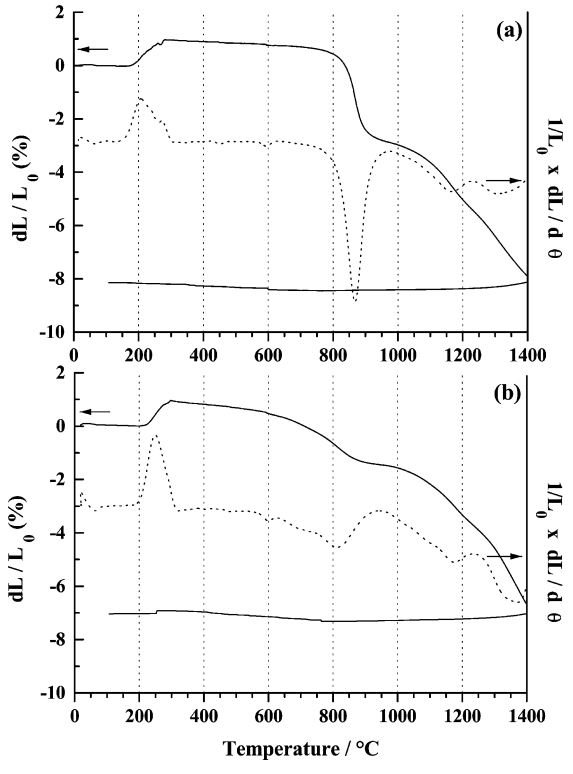

Fig. 6 Dilatometric curve of $GdPO_4$ (a) and $La_{0.5}Gd_{0.5}PO_4$ (b) ($P = 150$ MPa): relative shrinkage (solid line) and derivative $dL/d\theta$ (dotted line).

Table 6 Results of PIXE and EPMA analyses on sintered samples of $GdPO_4$

Sample	θ/°C	Time/h	Gd/wt. %	P/wt. %	O/wt. %	Gd/P
Calcd			62.3	12.3	25.4	1.00
PIXE	1300	5	62.1 ± 2.1	12.4 ± 0.4	25.5 ± 1.6	1.01 ± 0.07
EPMA	1300	12	60.1 ± 1.9	12.5 ± 0.4	27.4 ± 1.7	0.95 ± 0.06
EPMA	1250	12	62.1 ± 0.5	12.7 ± 0.2	25.2 ± 0.6	0.97 ± 0.03

Determination of the apparent and effective relative densities. The elaboration of sintered pellets of lanthanum–gadolinium monazites was developed using a two-step procedure based on a uniaxial pressing at room temperature between 200 and 700 MPa, followed by a final heat treatment at 1250 or 1300 °C for 10 to 180 h. This procedure was applied to the powder prepared after an initial heating at 400 °C (first method of synthesis) in order to achieve the elimination of the volatile products. All the pellets characterized using PIXE and/or EPMA (Table 6) appeared homogeneous and single phase. Moreover, the elementary weight percentage as well as the mole ratios were found to be in good agreement with those calculated from the empirical formula.

Either the apparent or the effective relative densities were determined for the sintered samples of monazite. The first value was obtained using water pycnometry while the second was determined using helium and water pycnometries after degassing of the sample. The results obtained on $GdPO_4$ pellets heated for 165 h at 1300 °C for several initial pressures are gathered in Table 7, while the evolution of the apparent and effective relative densities are reported in Fig. 7. For both temperatures considered (1250 and 1300 °C), the densification appeared rather good. Indeed, for initial pressures of 200–700 MPa, the relative effective density reached 95–99% of the value calculated from the XRD data. Moreover, for all the solids considered, the initial pressure did not have any significant influence on the final apparent and effective relative densities even though a weak influence was observed during the first hours of heating ($d_{app.}$ and $d_{eff.}$ reached 93–97% and 96–99% of d_{calcd} after heating between 5 and 20 h at 1300 °C). These results are consistent with those published by Boatner *et al.* who reported an effective relative density of 98% for $CePO_4$ prepared by hot pressing and after controlling the particle size by a urea precipitation process.[36] The densities were correlated to the specific area for several holding times. The main results are gathered in Fig. 8. For 140 h of heating time, the specific area was found to be 0.7–0.8 and 0.4 $m^2\ g^{-1}$ when heating at 1250 and 1300 °C, respectively. These values were rather low but remain higher than those measured for sintered samples of other phosphate matrices in pellet form, such as TPD (800–950 $cm^2\ g^{-1}$).[62]

Observation of the sintered samples by SEM. The observation of the sintered samples of $GdPO_4$ by SEM showed a rather good homogeneity in spite of several fractures (Fig. 9). These were probably generated by the elimination of volatile

Table 7 Variation of the apparent and effective relative densities of sintered $GdPO_4$ after heating for 165 h at 1300 °C *versus* the initial pressure

Initial pressure/MPa	200	400	600	700
Apparent relative density (water)/%	95 ± 2	95 ± 2	94 ± 2	96 ± 2
Effective relative density (water)/%	96 ± 2	96 ± 2	95 ± 2	96 ± 2
Effective relative density (He)/%	99 ± 1	99 ± 1	98 ± 1	98 ± 1
Open porosity/vol %	1–4	1–4	1–3	0–2
Closed porosity/vol %	1–4	1–4	2–5	2–4

Published on 15 May 2003 on http://pubs.rsc.org | doi:10.1039/B212805P
Downloaded on 26 October 2010

View Online

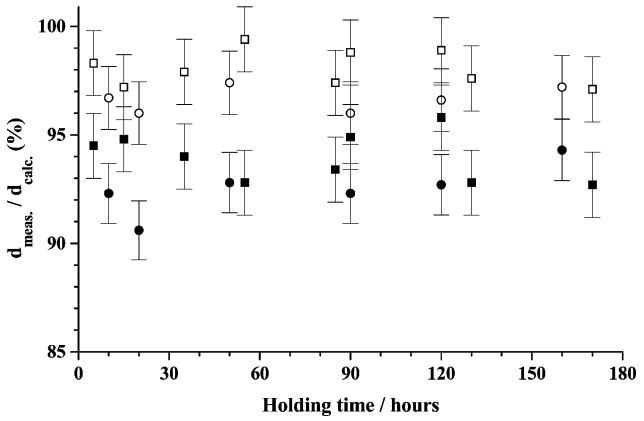

Fig. 7 Variation of the apparent (solid symbols) and effective (open symbols) relative densities of sintered samples of $GdPO_4$ after heating at 1250 (●/○) or 1300 (■/□) °C (initial pressing: 300 MPa).

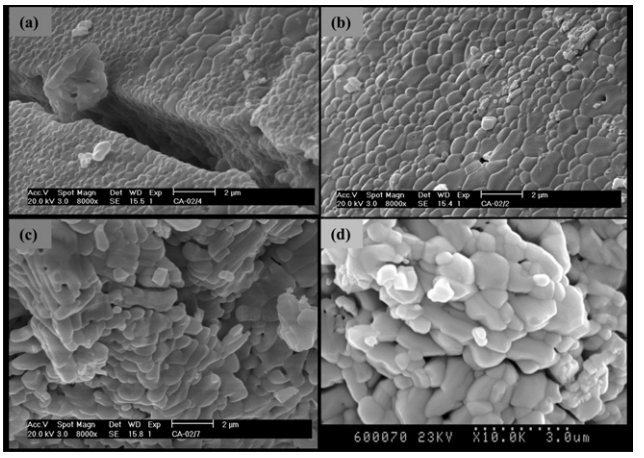

Fig. 9 SEM micrographs of sintered samples of $La_{1-x}Gd_xPO_4$ ($x = 0.8$ or 1.0) after heating at 1250 °C for 20 h: surface (a,b) and fractured material (c,d).

products (*e.g.*, water) occurring during the heat treatment. On the contrary, the surface of the sample appeared very dense: some rare intergranular and intragranular pores were detected while the grain boundaries were clearly observed. This average grain size was equal to about 1 μm. The inside of the pellet heated at 1250 °C exhibited some grains of 2 μm in length and 0.5 μm in width. The coalescence of these grains was clearly observed, leading to the formation of agglomerates of about 10 μm in length (this population, varying from 20 to 90 μm, with an average size of 10 μm, was evidenced in the grain size distribution).

Chemical durability of sintered samples of $GdPO_4$

In order to test the resistance of monazite-type $GdPO_4$ to aqueous alteration and to avoid the formation of neoformed phases (which could occur under the conditions of stored radioactive waste, *i.e.*, in groundwater, neutral or alkaline media), several sintered samples heated at 1300 °C (SA = 0.4 $m^2\ g^{-1}$) were leached in very aggressive acidic media (Table 8). The results obtained when leaching the solids at 90 °C in several media are reported in Fig. 10. During the first 5 days of leaching, the normalized leaching increased linearly with the leaching time, allowing a determination of the corresponding normalized dissolution rates. This behavior was also observed when leaching the samples at room temperature in 10^{-1}M HNO_3 ($R_H = 2.2 \pm 0.7 \times 10^{-5}$ g m^{-2} day^{-1}). From the values determined at 90 °C and room temperature, the apparent activation energy was evaluated to be 39–45 kJ mol^{-1}. The results reported in Table 8 are consistent with those given in the literature for natural monazites[37] and remained very low in comparison to those of other ceramics such as apatites, zircons, zirconolites, pyrochlore or synroc.[63–67] On the basis of these preliminary results, the dependence of the normalized dissolution rate with the pH was evaluated. From our results, the partial order related to the proton concentration at 90 °C was evaluated to be about 0.6, which is higher than that obtained for several other compounds such as TPD[24,25,68,69] or thorium–uranium(IV) dioxides.[70,71] For longer leaching times, the normalized leaching reached a plateau due to saturation of the leachate (establishment of a thermodynamic equilibrium with precipitated neoformed phosphate phase to rhabdophane-type $GdPO_4 \cdot 0.5H_2O$ under our experimental conditions).

Moreover, the neoformed phases were quickly precipitated, probably at the surface of the pellet as already described for thorium–uranium(IV) phosphate–diphosphate solid solutions.[72] Under these conditions, it was thus possible to determine the solubility product $K^{o}_{s,0}$ of $GdPO_4 \cdot 0.5H_2O$ at 90 °C and then at 20 °C. The first evaluation of the value of Log ($K^{o}_{s,0}$) was found to lie between −19.2 and −23.9 for leaching experiments performed in hydrochloric media and between −21.8 and −22.4 when working in nitric media. For the extrapolation of the solubility product to room temperature, the variation of the enthalpy of the reaction of precipitation of $NdPO_4 \cdot 0.5H_2O$ was considered. These values are of the same order of magnitude as those reported for amorphous $GdPO_4 \cdot xH_2O$ [Log ($K^{o*}_{s,0}$) = -25.39 ± 0.23].[73,74] Complementary calculations involving speciation programs such as CHESS[75] are now in progress to give more accurate values of the solubility products of the neoformed phases.

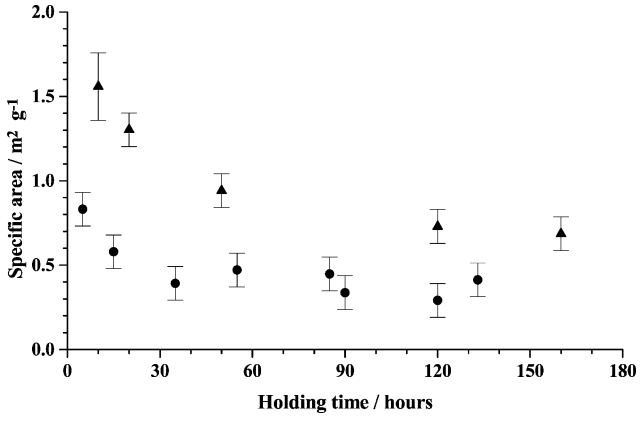

Fig. 8 Evolution of the specific area of sintered samples of $GdPO_4$ (initial pressing: 300 MPa) after heating at 1300 (●) or at 1250 (▲) °C.

Table 8 Normalized dissolution rate for Gd monazite in several acidic media

	R_L(M)/g m^{-2} day^{-1}		
	Natural monazite (M = Ce), θ = 70 °C[37]	Sintered $GdPO_4$ (M = Gd), θ = 90 °C	
pH	HCl	HCl	HNO_3
1	6×10^{-4}	$(3.8 \pm 0.8) \times 10^{-4}$	$(5.9 \pm 2.1) \times 10^{-4}$
2	$2–3.2 \times 10^{-5}$	N.D.[a]	N.D.
2.6	7×10^{-6}	N.D.	N.D.
4	N.D.	$(4.8 \pm 1.4) \times 10^{-6}$	N.D.
6	8×10^{-7}	N.D.	N.D.

[a] N.D. = not determinded.

Published on 15 May 2003 on http://pubs.rsc.org | doi:10.1039/B212805P
Downloaded on 26 October 2010

View Online

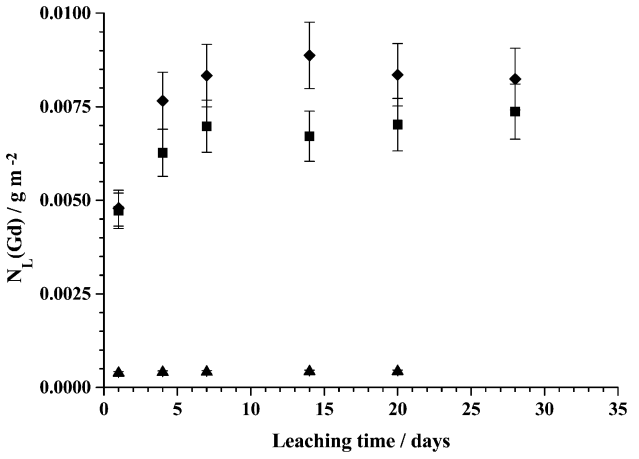

Fig. 10 Evolution of the normalized leaching N_L(Gd) with time when leaching sintered samples of $GdPO_4$ in 10^{-1}M HNO_3 (◆), 10^{-1}M HCl (■) and 10^{-4} M HCl (▲) at $\theta = 90\,^{\circ}C$.

Conclusions

The results reported in this paper allowed us to confirm the good properties of monazites for the immobilization of radioactive waste and especially for trivalent actinides. Indeed, the solid solutions of $La_{1-x}Gd_xPO_4$ exhibit good sintering properties and a high resistance to aqueous alteration ($R_L = 10^{-6}$ to 10^{-4} g m^{-2} day^{-1}) even in acidic media. In the back-end of the initial dissolution of monazites, two kinds of neoformed phases should delay the migration of trivalent actinides when performing the leaching tests at 150 °C in closed containers.

Although lanthanum and cerium are precipitated at 150 °C as a monazite-type compounds, praseodymium forms simultaneously both phases (rhabdophane and monazite types). From neodymium to dysprosium, the rhabdophane $MPO_4{\cdot}0.5H_2O$ was prepared, while from holmium to lutetium, the precipitated phase crystallized in the tetragonal system of the churchite-type structure. On the basis of this study and considering their ionic radii, both americium and curium [$^{VIII}r(An^{3+}) = 1.09$ Å][33] should be rapidly precipitated as $AnPO_4{\cdot}0.5H_2O$ (in the rhabdophane-type structure), leading to a very low radioactivity release in the leachate as already suggested from the leaching tests performed over several years on thorium phosphate diphosphate doped with ^{241}Am and ^{244}Cm.[25]

Taking into account the very good properties of monazite MPO_4 (dedicated to the immobilization of An^{3+}) and thorium phosphate diphosphate (synthesized with the aim to immobilize An^{4+}), the preparation, characterization, sintering and the chemical durability of $Th_{4-x}U_xP_6O_{23}/MPO_4$ (M = La, Nd, Gd) based composites are now under study. The first results show that several properties of interest of TPD and monazites (like easy preparation and sintering, densification, chemical durability and retention properties by rapid precipitation of low-soluble neoformed phases) are conserved in these composite materials. Several results related to the elaboration, the sintering, and the chemical durability of these solids will be published soon.

Acknowledgements

The authors would like to thank Lionel Aranda, Frédéric Diot, Jean-Paul Emeraux and Alain Kohler from the LCSM of the University Henri Poincaré of Nancy (France) for the EPMA analyses, the XRD and TGA/DTA experiments, the SEM observations and for the dilatometry study.

The authors would like also to thank Gerard Lagarde from IPN-Orsay (France) and Joseph Salomon from LMRF (Palais du Louvre, France) for performing the PIXE experiments and are very grateful to Professor Didier Bernache from University of Limoges (France) for his help in the understanding of the dilatometry study

References

1 L. A. Boatner and B. C. Sales, in *Radioactive Waste Forms for the Future*, eds. W. Lutze and R. C. Ewing, North-Holland Physics Publishing, Amsterdam, 1998, p. 495.
2 R. Podor and M. Cuney, *Am. Mineral.*, 1997, **82**, 765.
3 R. Podor, M. Cuney and C. Nguyen Trung, *Am. Mineral.*, 1995, **80**, 1261.
4 A. Meldrum, L. A. Boatner, W. J. Weber and R. C. Ewing, *Geochim. Cosmochim. Acta*, 1998, **62**, 2509.
5 M. Petek, M. M. Abraham and L. A. Boatner, in *The Scientific Basis for Nuclear Waste Management*, Materials Research Society, Pittsburgh, PA, USA, 1982, p. 181.
6 R. J. Floran, M. M. Abraham, L. A. Boatner and M. Rappaz, in *Scientific Basis for Nuclear Waste Management*, Materials Research Society, Pittsburgh, PA, USA, 1980, vol. 3, p. 507.
7 M. M. Abraham, L. A. Boatner, T. C. Quinby, D. K. Thomas and M. Rappaz, in *Radioactive Waste Management*, Materials Research Society, Pittsburgh, PA, USA, 1980, vol. 1, p. 181.
8 J. M. Montel, J. L. Devidal and D. Avignant, *Chem. Geol.*, 2002, **191**, 89.
9 J. Carpena, F. Audubert, D. Bernache, L. Boyer, B. Donazzon, J. L. Lacout and N. Senamaud, in *Scientific Basis for Nuclear Waste Management XXI*, eds. I. G. McKinley and C. McCombie, Materials Research Society, Warrendale, PA, USA, 1998, vol. 506, p. 543.
10 F. Audubert, J. Carpena, J. L. Lacout and F. Tetard, *Solid State Ionics*, 1997, **95**, 113.
11 R. Bros, J. Carpena, V. Sere and A. Beltritti, *Radiochim. Acta*, 1996, **74**, 277.
12 H. T. Hawkins, B. E. Scheetz and G. D. Guthrie, Jr., *Mater. Res. Soc Symp. Proc.*, 1996, **465**, 387.
13 H. T. Hawkins, D. R. Spearing and G. D. Guthrie, Jr., *Chem. Mater.*, 1999, **11**, 2851.
14 S. Nakayama and K. Itoh, *J. Eur. Ceram. Soc.*, 2003, **23**, 1047.
15 A. I. Orlova, Y. F. Volkov, R. F. Melkaya, L. Y. Masterova, I. A. Kulikov and V. A. Alferov, *Radiokhimiya*, 1994, **36**, 322.
16 L. Bois, M. J. Guittet, F. Carrot, P. Trocellier and M. Gautier-Soyer, *J. Nucl. Mater.*, 2001, **297**, 129.
17 R. Drot, C. Lindecker, B. Fourest and E. Simoni, *New. J. Chem.*, 1998, **22**, 1105.
18 P. Benard, V. Brandel, N. Dacheux, S. Jaulmes, S. Launay, C. Lindecker, M. Genet, D. Louër and M. Quarton, *Chem. Mater.*, 1996, **8**, 181.
19 V. Brandel, N. Dacheux and M. Genet, *Radiokhimiyia*, 2001, **43**, 16.
20 N. Dacheux, Ph.D. Thesis, Université Paris XI, Orsay, 1995 (IPNO-T-95.04).
21 N. Dacheux, R. Podor, B. Chassigneux, V. Brandel and M. Genet, *J. Alloys Compd.*, 1998, **271**, 236.
22 N. Dacheux, R. Podor, V. Brandel and M. Genet, *J. Nucl. Mater.*, 1998, **252**, 179.
23 N. Dacheux, A. C. Thomas, V. Brandel and M. Genet, *J. Nucl. Mater.*, 1998, **257**, 108.
24 A. C. Thomas, Ph.D. Thesis, Université Paris XI, Orsay, 2000 (IPNO-T-00.09).
25 A. C. Robisson, N. Dacheux and J. Aupiais, *J. Nucl. Mater.*, 2002, **306**, 134.
26 P. Benard, D. Louër, N. Dacheux, V. Brandel and M. Genet, *Chem. Mater.*, 1994, **6**, 1049.
27 P. Benard, D. Louër, N. Dacheux, V. Brandel and M. Genet, *An. Quim., Int. Ed.*, 1996, **92**, 79.
28 V. Brandel, N. Dacheux, J. Rousselle and M. Genet, *C.R. Acad. Sci., Chim.*, 2002, **121**, 467.
29 V. Brandel, N. Dacheux and M. Genet, *J. Solid State Chem.*, 1996, **5**, 1.
30 K. L. Kelly, G. W. Beall, J. P. Young and L. A. Boatner, in *Scientific Basis for Nuclear Waste Management*, ed. J. G. Moore, Materials Research Society, Warrendale, PA, USA, 1980, vol. 3, 189.
31 A. S. Aloy, E. N. Kovarskaya, T. I. Kolsova, S. E. Samoylov, S. I. Rovnyi, G. M. Medvedev and L. J. Jardine, in *Proceedings of the 10th International Ceramics Congress*, American Society of Mechanical Engineers (ASME), New York, USA, 2002 (CD-ROM).

Published on 15 May 2003 on http://pubs.rsc.org | doi:10.1039/B212805P
Downloaded on 26 October 2010

View Online

32 D. D. Davis, E. R. Vance and G. J. McCarthy, in *Scientific Basis for Nuclear Waste Management*, ed. J. G. Moore,Materials Research Society, Warrendale, PA, USA, 1980, vol. 3, 197.
33 R. D. Shannon, *Acta Crystallogr.*, 1975, **5**, 186.
34 R. Podor, M. François and N. Dacheux, *J. Solid State Chem.*, 2003, **172**, 66.
35 A. Tabuteau, M. Pages, J. Livet and C. Musikas, *J. Mater. Sci. Lett.*, 1988, **7**, 1315.
36 L. A. Boatner, G. W. Beall, M. M. Abraham, C. B. Finch, P. G. Huray and M. Rappaz, in *Scientific Basis for Nuclear Waste Management*, ed. C. J. M. Northrup, Jr., Materials Research Society, Warrendale, PA, USA, 1981, vol. 2, p. 289.
37 E. H. Oelkers and F. Poitrasson, *Chem. Geol.*, 2002, **191**, 73.
38 Y. Eyal and D. R. Olander, *Geochim. Cosmochim. Acta*, 1990, **54**, 1867.
39 D. R. Olander and Y. Eyal, *Geochim. Cosmochim. Acta*, 1990, **54**, 1879.
40 D. R. Olander and Y. Eyal, *Geochim. Cosmochim. Acta*, 1990, **54**, 1889.
41 G. Charlot and D. Bezier, *Analyse Quantitative Minérale*, Masson, Paris, France, 1955.
42 S. Brunauer, P. H. Emmet and E. Teller, *J. Am. Chem. Soc.*, 1938, **60**, 309.
43 W. O. Milligan and D. F. Mullica, *Acta. Crystallogr., Sect. C*, 1983, **39**, 23.
44 Y. X. Ni, J. M. Hughes and A. N. Mariano, *Am. Mineral.*, 1995, **80**, 21.
45 A. Hezel and S. D. Ross, *J. Inorg. Nucl. Chem.*, 1967, **29**, 2085.
46 Y. Hikichi, K. Yogi and T. Ota, *J. Alloys Compd.*, 1995, **224**, L1.
47 *Powder Diffraction File™ (Database)*, International Centre for Diffraction Data, Newton Square, PA, USA, 2001.
48 M. Evain, *U-Fit Program*, Institut des Matériaux de Nantes, France, 1992.
49 B. Scheetz, in *Powder Diffraction File™ (Database)*, International Centre for Diffraction Data, Newton Square, PA, USA2001, JCPDS File no 39–0232.
50 R. C. L. Mooney, *J. Chem. Phys.*, 1948, **16**, 1003.
51 T. Uedo, *J. Jpn. Assoc. Mineral. Petrol. Econ. Geol.*, 1967, **58**, 170.
52 F. Weigel, V. Scherer and H. Henschel, *Radiochim. Acta*, 1965, **4**, 18.
53 S. Kirik, L. Solovyov, A. Blokhin and R. Mulagaleev, in *Powder Diffraction File™ (Database)*, International Centre for Diffraction Data, Newton Square, PA, USA,2001 JCPDS File no 50–0620.
54 H. Schwarz, *Z. Anorg. Allg. Chem.*, 1963, **323**, 44.
55 R. G. Jonasson and E. R. Vance, *Thermochim. Acta*, 1986, **108**, 65.
56 H. Onoda, H. Nariai, H. Maki and I. Motooka, *Mater. Chem. Phys.*, 2002, **73**, 19.
57 I. Horvath, I. A. Bondar and L. P. Mezentseva, *J. Therm. Anal.*, 1988, **33**, 755.
58 Y. Hikichi, T. Sasaki, K. Murayama, T. Nomura and M. Miyamoto, *J. Am. Ceram. Soc.*, 1989, **72**, 1073.
59 R. C. L. Mooney, *Acta Crystallogr.*, 1950, **3**, 337.
60 Y. Hikichi, K. Hukuo and J. Shiokawa, *Bull. Chem. Soc. Jpn.*, 1978, **51**, 3645.
61 M. Zaki, A. Aamili, A. Sadel, M. Zahir, M. El-Ghozzi and D. Avignant, *Ann. Chim. Sci. Mater.*, 2001, **26**, 35.
62 N. Dacheux, B. Chassigneux, V. Brandel, P. Le Coustumer, M. Genet and G. Cizeron, *Chem. Mater.*, 2002, **14**, 2953.
63 E. Valsami-Jones, K. V. Radnagsttodir, A. Outnis, D. Bosbach, A. J. Kemp and G. Cressey, *Chem. Biol.*, 1998, **151**, 215.
64 K. B. Helean, W. Lutze and R. C. Ewing, in *Environmental Issues and Waste Management Technologies in the Ceramic and Nuclear Industries IV*, ed. G. T. Chandler, American Ceramic Society, Westerville, Ohio, USA, 1999, vol. 93, 297.
65 P. Mc Glinn, K. P. Hart, E. H. Loi and E. R. Vance, in *Scientific Basis for Nuclear Waste Management*, eds. T. Murakami and R. C. Ewing, Materials Research Society, Pittsburgh, PA, USA, 1994, vol. 353, 847.
66 K. P. Hart, Y. Zhang, E. Loi, Z. Aly, M. W. A. Stewart, A. Brownscombe, B. B. Ebbinghaus and W. Bourcier, in *Scientific Basis for Nuclear Waste Management XXIII*, eds. R. W. Smith and D. W. Shoesmith, Materials Research Society, Warrendale, PA, USA, 2000, vol. 608, 353.
67 K. P. Hart, E. R. Vance, R. Stanojevic and R. A. Day, in *Scientific Basis for Nuclear Waste Management XXII*, eds. D. J. Wronkiewicz and J. H. Lee, Materials Research Society, Warrendale, PA, USA, 1999, vol. 556, 173.
68 A. C. Thomas, N. Dacheux, P. Le Coustumer, V. Brandel and M. Genet, *J. Nucl. Mater.*, 2000, **281**, 91.
69 A. C. Thomas, N. Dacheux, P. Le Coustumer, V. Brandel and M. Genet, *J. Nucl. Mater.*, 2001, **295**, 249.
70 S. Hubert, K. Barthelet, B. Fourest, G. Lagarde, N. Dacheux and N. Baglan, *J. Nucl. Mater.*, 2001, **297**, 206.
71 G. Heisbourg, S. Hubert, N. Dacheux and J. Ritt, *J. Nucl. Mater.*, 2003 , in press.
72 N. Clavier, N. Dacheux, O. Terra, P. Le Coustumer and R. Podor, in *Proceedings of the 10th International Ceramics Congress*, ed. P. Vincenzini, Techna Srl, Faenza, Italy, 2003, vol. 33, 209.
73 H. Firscing and S. Brune, *J. Chem. Eng. Data*, 1991, **36**, 93.
74 H. Firscing and J. Kell, *J. Chem. Eng. Data*, 1993, **38**, 132.
75 J. Van der Lee de Windt, *CHESS Tutorial and Cookbook*, Ecole des Mines de Paris, Fontainebleau, 1999 (LHM/RD/99/05).

Published on 15 May 2003 on http://pubs.rsc.org | doi:10.1039/B212805P
Downloaded on 26 October 2010